Characterization of polymer materials using FT-IR and DSC techniques

Pere Pagès
Departamento de Ciencia de Materiales, Universitat Politècnica de Catalunya. Colom, 11, 08222-Terrassa. Spain
pedro.pages@upc.es

1. Introduction

In this chapter the autor realise various studies about the structural characterisation of polymer materials, using the Infrared spectrophotometry (FT-IR) and the Differential Scanning Calorimetry (DSC) techniques.

Results obtained by means of both techniques are in all the cases complementaries in order to achieve a better comprensiveness about the structure of the polymers.

2. Part one: FT-IR and DSC study of HDPE structural changes and mechanical properties variation when exposed to weathering aging during canadian winter

This work studies the influence of the climatic conditions during the Canadian winter using high-density PE (HDPE) samples exposed to weather conditions during different periods of time. Under these conditions, it is reasonable to think that the chemical changes caused by the climatic degradation will at first sight be due to photochemical reactions (sunlight) and, to a lesser extent, to hydrolytic reactions (environmental moisture). FT-IR was used to study the microstructural changes. Similarly, many of these microestructural modifications are thought to originate some changes in the crystalline content. As is well known, crystallinity is closely related to the macroscopic properties of the polymer and this knowledge is fundamental in engineering applications. Therefore, another objective of this work is the study of the crystallinity variation of the polymer subjected to drastic environmental conditions by using two techniques: FTIR and DSC. The variation of the mechanical properties of HDPE exposed to the indicated climated conditions was also analyzed.

2.1. Experimental

2.1.1. Materials

HDPE (HDPE 2909, Du Pont Canada) is a thermoplastic polymer with the following properties: density 960 kg/m^3 and melting flow index 1.35 g/min.

2.1.2. Preparation of HDPE Samples

Samples were prepared in a mold according to ASTM D-638 (type V). The HDPE, previously milled and screened, was compacted in a mold at 3 MPa pressure for 20 min at room temperature. Then it was heated to 150^{0}C and pressure increased to 3.2 MPa for 20 min. Demolding was accomplished by slowly quenching the mold until room temperature to prevent bubble formation.

2.1.3. Environmental Conditions

Samples were weather exposed during different periods of time: 0, 15, 30, 60 and 90 days. Figure 1 shows the daily data about minimum and maximum temperatures during the time studied. In addition to the low temperatures there is a very accentuated difference of temperature between day and night (i.e., thermal fatigue). As a result, treatments can be considered as doubly drastic.

2.1.4. Analytical Techniques

Microstructural changes in the HDPE were determined by FTIR spectrophotometry. In relation to the variation of crystallinity, two instrumental analytical techniques were used: FTIR and DSC.

FTIR Spectrophotometry

A Nicolet 510 M with CsI optics was used to obtain the FTIR spectra. The method to prepare the samples consisted of dispersing the surface of the finely divided sample (9 mg) in a matrix of KBr (300 mg), followed by compression at 167 MPa to compact the pellet.

To evaluate microstructural changes undergone by the HDPE samples, the pertinent spectra were obtained for each of the treatment periods (from 0 to 90 days). Based on the spectral recordings, called "basic," the variations that occurred were analyzed: formation/disappearance, increase/decrease, and displacement of the various bands. To evaluate these differences, subtraction between the various spectra was used by enlarging the spectrum zones that give better information, 775-1540 and 1600-1800 cm [1].

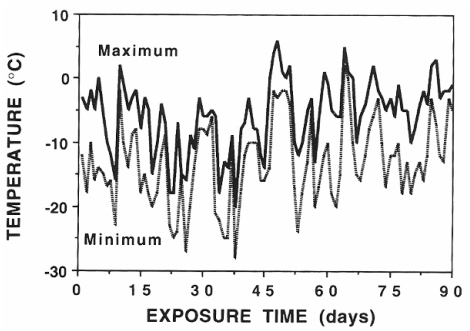

Figure 1. Maximum and minimum values of HDPE temperature during the exposure period to environmental conditions.

These zones include and surpass the spectral zones used in previous works to study the PE aging [2].

Concerning the crystallinity, the literature indicates that it was first determined by the ratio of the absorption intensities at 1303 cm^{-1} corresponding to the amorphous phase of the solid and melted states [7]. This method implies incertitude as the absorption coefficients in both states are not the same. A procedure based on a universal calibration constant and on the measure of the absorption intensity at 1303 cm^{-1} of the amorphous phase was later developed. Unfortunately, this method can only be applied if the film density and thickness are known [8].

Zerbi et al. [9] recently suggested the use of spectral bands corresponding to the bending vibrations: 1474 and 730 cm^{-1} (crystalline phase) and 1464 and 720 cm^{-1} (amorphous phase). This procedure was selected for this work as the preparation technique in pellets provides intense absorptions in such spectral bands while the absorption at 1303 cm^{-1} gives low intensity due to the high crystallinity of the HDPE. Therefore, mainly two spectral zones were analysed:

600-800 cm^{-1} (containing the bands 720 and 730 cm^{-1}) and 1400-1550 cm^{-1} (containing the bands 1464 and 1474 cm^{-1}).

DSC

This technique was used to support the results of crystallinity obtained by FTIR. A DSC 30 Mettler analyzer, with liquid nitrogen, capable of reaching a maximum sensitiveness of 0.4 mJ/s per each 100 divisions of the recording paper was used to obtain the thermograms. The sample weight varied between 2.0 and 3.0 mg. Weights sufficiently small were selected to prevent heat transfer problems, such as was already proved in previous thermogravimetric studies [10]. The heating rate was 20 K/min, which means a balanced compromise between the measuring speed and the peak resolution. The temperature range analysed was 50-200ºC. The temperature and energy calibration was achieved by means of In, Pb, and Zn standards, under identical analytical conditions of the HDPE samples.

2.1.5. Mechanical Properties

The tensile strength, elasticity modulus, and impact energy were determined by standardized procedures to study the influence of aging on the mechanical properties.

2.1.6. Analysis of Chemical Changes

With the spectral subtractions of the different samples exposed during various periods of time, taking as reference the nondegradated HDPE sample, tables were prepared in which the most relevant results are shown. Table 1 shows the most significant bands studied and their distinctive functional group. Table 2 defines the behavior of all the bands specified that are listed according to generated, transformed, or invariable functional groups as the result of the exposure undergone during a period of 15 days. The progress of the microstructural phenomena of configuration as the exposure time increased is shown in Table 3.

A comparative study with the results found by D'Esposito and Koening [2] shows a significant coincidence in most of the bands studied, although some discrepant bands also occur. These discrepant values are corroborated by characteristic and original bands pertaining to the region of 1700-1800 cm^{-1} that were not included in the above-mentioned work, even though these bands are confirmatory of groups obtained within the range 750-1425 cm^{-1}.

Table 1. Spectral FTIR Bands Studied

	Wave Number (cm^{-1})	**Functional Groups**	**Type of Vibration**
(1)	900	$RR'C=CH_2$	C-H rocking
(2)	909	$RCH=CH_2$	C-CH_2 out of plane bending
(3)	971	(trans) R'CH=CHR	=C-CH bending, R and R' are alkyl groups
(4)	990	$RCH=CH_2$	=C-H out of plane bending, related to (2)
(5)	1068	RCH_2-CHOH-CH_2R'	C-O stretching, corresponding to a secondary alcohol, R and R' are groups with insaturations
(6)	1131	RCH_2-COH(CH_3)-CH_2-	C-O stretching,corresponding to a tertiary alcohol
(7)	1177	-$CH(CH_3)_2$	C-C stretching and C-C-H bending
(8)	1368	-$C(CH_3)_3$	Doblet in C-H bending
(9)	1360	-CO-CH_3	-CH_3 symmetric vibration in a ether
(10)	1375	-CH_3	C-H symmetric bending
(11)	1410	RCH_2-CO-CH_2R	-CH_2- scissoring
(12)	1653	(cis) R'CH=CHR	Terminal bond vibration where R and R' are alkyl chains
(13)	1692	R-CO-OR'	C=C stretching where R and R' are vinyl groups
(14)	1738	R-CO-OR'	C=O stretching where R and R' are alkyl groups

Table 2 Functional Groups Resulting from HDPE Aging for 15-Day Exposure Time (by FTIR)

	Spectral Bands (cm^{-1})	**Generated Groups**
(7)	1177	$-CH(CH_3)_2$
(8)	1368	$-C(CH_3)_3$
(9)	1360	$-CO-CH_3$
(10)	1374	$-CH_3$
(11)	1410	$R-CH_2-CO-CH_2-R'$
(13)	1692	R-CO-OR'
(14)	1738	R-CO-OR'
(2)	909	$R-CH=CH_2$
(12)	1653	RHC=CHR' (cis), terminal insaturations related to (2) Unchanged Groups
(1)	900	$R'RC=CH_2$
(3)	971	(trans) RCH=CHR'
(4)	990	$RCH=CH_2$
(5)	1068	$RCH_2-CHOH-CH_2R'$
(6)	1131	$-CH_2-C(CH_2R)OH-CH_2$

Table 3 Types of Spectral Bands Resulting from HDPE Aging for 15, 60, and 90-Day Exposure Time to Environmental Conditions (by FTIR)

15 Days		
Intensity Increase, Generated groups (cm^{-1})	**Intensity Increase, Transformed Groups (cm^{-1})**	**Unchanged Intensity (cm^{-1})**
900, 1177, 1368, 1375, 1360, 1410, 1692, 1738	909, 990, 1953	971, 1068, 1131
60 Days		
900,971,1368,1375,1360, 1131,1692,1738	909,990,1068,1683	1177,1410
90 Days		
900,971,1368,1375,1360, 1131,1692,1738	909,990,1068,1653	1177,1410

On comparing the results of the first 15 and 30 days of exposure, the trend followed by the increase bands (generation of groups) and the decrease bands (transformation of groups) remain unchanged. Bands at 900 and 990 cm^{-1} initially belonging to the invariant group are incorporated, respectively, to the increase and decrease blocks. Results at 60-days degradation confirm the previously mentioned values. The characteristic block of transformed groups was increased by the incorporation of an invariant band while the characteristic block of generated groups did not change. In view of these results, it was confirmed that the microstructural changes undergo alterations during the first 60 days of exposure, thus becoming stable.

The results confirm the microstructural configuration modifications occurring in the polymeric chains. Such modifications are defined by a series of mechanisms involved in the HDPE degradation:

1. *chain breaking* with the formation of characteristic groups (methyl, terbutyl, iaopropyl, and end insaturations) due to homolytic and heterolytic dissociations reflected in the positive evolution banda (900, 1177, 1368, 1375, and 1678 cm^{-1});
2. *chain branching* with generated groups defined by bands 1177, 1368, and 1375 cm^{-1} and with transformed groups (909, 990, and 1653 cm^{-1}) that confirm these modifications;
3. *crosslinks* between polymeric chains caused by additive reactions on double linkages. The characteristic groups defining this type of modification appear in the negative evolution bands (909 and 1653 cm^{-1});
4. *oxidation phenomena* defined by the positive evolution bands (1760, 1410, 1692, and 1675 cm^{-1}) and involving the formation of peroxides, alcohol groups, and carboxylic groups.

To summarize this study, Table 4 shows the evolution of the different characteristic bands that define every phenomenon occurring in the configurational variations and their relationships to the various exposure times.

2.1.7. Crystallinity Variation

The empirical relation proposed by Zerbi et al. [9] was used to evaluate crystallinity:

$$X = \frac{\frac{1 - I_a / I_b}{1.233}}{1 + \frac{I_a}{I_b}}.100$$

where X is the percentage of the amorphous content, I_a and I_b the intensities of absorption in the bands of 730 and 720 cm^{-1} or, alternatively, at 1474 and 1464 cm^{-1}, respectively. The constant 1.233 corresponds to the relations of intensity bands of fully crystalline HDPE.

Table 5 illustrates the variation of the HDPE amorphous and crystalline content as a function of the exposure time and the calorimetric features (initial and final melting temperatures and the melting enthalpy). Results show relevant discrepancies according to the spectral bands selected for the evaluation of the content in both the amorphous and crystalline phases. The intensity ratio 730/720 cm^{-1} leads to random results for crystallinity without the possibility of establishing the level of degradation in terms of

its duration. In addition, the crystallinity varies in the range 71.5-76.6%, values too low for the HDPE, which is a highly crystalline polymer. The density and also the melt flow index of HDPE confirm that it is a material prepared with a Phillips-type catalyst, whose crystallinity is around 90% [11]. The conclusion from these facts is that the measurement of crystallinity through the bands 730/ 720 cm^{-1} is not adequate. On the contrary, the bands 1474/1464 cm^{-1} indicates that the crystallinity progressively decreases, while the weathering exposure time increases, from 98 to 95%. Moreover, these values are rather similar to the HDPE ones of this study. On the other hand, the calorimetry study that follows supports the validity of using the bands 1474/1464 cm^{-1}. In effect, from the thermograms obtained it is clear (see Table 5) the melting enthalpy decreases (i.e., crystallinity decrease) as the exposure time increases. This article has demonstrated that aging is caused by specific chemical transformations undergone by the polymeric chains.

Table 4 HDPE Microstructural Variations as a Function of Exposure Time (by FTIR)

Chains Breaking					
Days	900 cm^{-1}	971 cm^{-1}	1177 cm^{-1}	1368 cm^{-1}	1374 cm^{-1}
15	inv	inv	+	++	inv
30	+	inv	+	++	+
60	++	+	±	++	++
90	++	++	±	++	++

Chain Branching								
	900	909	971	990	1177	1368	1374	1653
15	inv	-	inv	inv	+	++	inv	---
30	+	--	inv	-	+	++	+	---
60	++	---	+	-	±	++	++	--
90	++	---	++	-	±	++	++	-

Oxidation Phenomena				
	1360 cm^{-1}	1410 cm^{-1}	1692 cm^{-1}	1738 cm^{-1}
15	+	+	++	++
30	++	+	+++	++
60	+++	±	+++	++
90	++	±	++	+++

Inv, unchanged; (+) increase; (-) decrease; (±) slight increase.

These reactive phenomena decrease the linear character of the polymeric chains caused by the formation of bulky groups, which leads to an increase of the amorphous content. Therefore, the crystallinity results found by DSC are in accordance with those recorded by FTIR in the bands 1474/1464 cm^{-1}. Figure 2 proves the actual linear relation between the melting enthalpy and the HDPE crystallinity degree. This correlation indicates that per each 1% of less crystallinity due to the aging process, the melting enthalpy decreases by 3.8 J/g. By extrapolation of the straight line at 100% crystallinity, a melting enthalpy of 229.0 J/g is obtained, corresponding to the fully crystalline HDPE.

Table 5 Variation of HDPE Amorphous and Crystalline Contents (by FTIR), Temperatures, and Melting Enthalpy (by DSC) as a Function of Exposure Time

Spectral Bands						
	I_a= 730 cm^{-1} I_b= 720 cm^{-1}		**I_a=1474 cm^{-1} I_b=1464 cm^{-1}**		Initial and Melting Temperatures (ºC)	Melting Enthalpy (J/g)
Exposure Time (Days)	Amorphous Content (%)	Crystalline Content (%)	Amorphous Content (%)	Crystalline Content (%)		
0	28.10	71.90	2.02	97.98	126.7-149.8	221.4
15	28.52	71.48	3.76	96.24	127.3-145.9	215.3
30	26.98	73.02	4.16	95.84	127.1-145.2	212.8
60	26.35	73.65	4.80	95.20	126.3-145.7	211.2
90	27.38	72.62	4.88	95.12	123.6-142.1	210.7

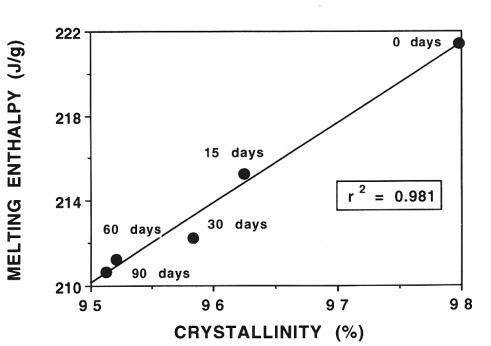

Figure 2 Relation between melting enthalpy and crystallinity of HDPE.

Table 6 shows the evolution of the mechanical properties studied. The decrease of the impact energy caused by the formation of bulky groups, imparting stiffness to the polymeric chains, is remarkable. The rest of the mechanical properties evaluated (tensile strength and Young's modulus) do not vary significantly with exposure, something to be expected as their characteristics basically depend on crystallinity. To be noted is that the HDPE crystallinity varies not more than 3% (environmental exposure of 90 days).

2.2. Conclusions part one

HDPE undergoes aging when submitted to drastic climatic conditions such as the Canadian winter: low temperature and sharp temperature changes between day and night (i.e., intense thermal fatigue). This aging becomes apparent by a series of chemical changes in the polymeric chains and a progressive decrease of HDPE crystallinity if the weathering exposure time increases.

The study of the spectral bands of samples degradated during different weathering exposure times demonstrated the existence of a series of microstructural modifications: chain breaking, chain branching, crosslinking, and oxidation. These configuration changes obviously influence the polymer crystallinity that was evaluated by quantifying the absorption intensity FTIR in two spectral bands: one characteristic of the amorphous phase and another of the crystalline phase. Two zones of the spectrum corresponding to vibrations of deformation, 730/720 cm^{-1} and 1474/1464 cm^{-1} were analyzed. The use of the bands 1474/1464 cm^{-1} was appropriate for the evaluation of crystallinity while the bands 730/720 cm^{-1} yielded random and too low results (71-77% with respect to the values that should be obtained for HDPE prepared with a Phillips-type catalyst, usually higher than 90%). Consequently, the use of the latter bands to evaluate the percentage of the polymer crystalline character was rejected. The results of DSC ratify the results accomplished by FTIR at 1474/1464 cm^{-1}, as the melting enthalpy, and therefore crystallinity, decrease with the weathering exposure time. Similarly, a linear relation between the melting enthalpy and crystallinity was made evident in such a way that 1% less crystallinity involves a 38 J/g decrease of the melting enthalpy. By application of this straight line and extrapolation at 100% crystallinity, a value of 229.0 J/g for the melting enthalpy was found, which should correspond to an ideal, fully crystalline HDPE. The property most affected by aging phenomena is the impact energy owing to the stiffness of the polymeric chains. The other mechanical properties evaluated (tensile strength and elasticity modulus) remain almost constant as they basically depend on the crystalline content of the polymer that decreases approximately 3% after 90 days of weathering exposure.

Table 6 Variation of HDPE Mechanical Properties as a Function of Exposure Time

Exposure Time (Days)	Tensile Strength (MPa)	Young's Modulus (GPa)	Impact Energy (mJ)
0	23.1	1.46	80.6
15	24.5	1.49	70.2
30	22.6	1.53	64.9
60	22.6	1.52	41.9
90	23.6	1.40	37.7

3. Part two: natural and artificial aging of polypropylene-polyethylene copolymers

It is known that exposing polymeric materials to environmental and artificial atmospheres changes their properties and external appearances with some modification of their surfaces. Several chemical reactions, induced by irradiation with sunlight, take place because of the chromophoric groups present in the polymer and the consequent ability of the polymer to absorb ultraviolet light Photoreactions are usually induced when polymer materials are damaged, causing embrittlement and color changes [12-14]. For the prevention of these phenomena, several methods have been developed. One of the most important is stabilizing the polymers with additives (i.e., antioxidants and light stabilizers).

To develop effective formulations, we must first know the causes and mechanism of the degradation. Fourier transform infrared (FTIR), differential scanning calorimetry (DSC), and scanning electron microscopy (SEM) are techniques used to evaluate the degradation process of polymeric materials. One of the earliest works performed with FTIR spectrophotometry was based on a study of PFT films exposed to high temperatures [15]. More recently, several studies on the artificial aging of different polymers were carried out, and their effects were quantified by FTIR spectrophotometry and photoacoustic FTIR [14, 16-18].

In this article, we report on aging-induced changes in the structural and thermal properties of polypropylene (PP)-polyethylene (PP)-based copolymers that were used as seats in the Olympic stadium of Barcelona, Spain. The samples were exposed to natural aging by weather for 2.5 years and to artificial aging by exposure to radiation from a xenon lamp for 5000 h, which is considered to be equivalent to 2.5 years of environmental exposure [19].

3.1. Experimental

The analyzed material was a PP-rich (~95 wt %) PP-PE copolymer manufactured by Repsol and marketed as PB 140. It was a block copolymer with short PE chains grafted to PP. The composition (95% PP) was chosen for its mechanical properties, that is, the high degree of toughness. Several additives were added to the base material. Table 7 shows a list of the various samples, which differed in the types and quantities of the additives employed.

The additives were antioxidants (Tinuvin 770, Irganox BZ15, Bioxid Kronos CL 2220, and Quimasorb 944) and colorants (blue Cromoftal A3R, red Cromoftal DPP-BO, violet Cinquasia R RT 891D, Iagacolor 10401, Byferrox 110, and Iagacolor 415).

Table 7. Description of the Additives Present in the Studied Copolymers

Sample	Additives
A	Tinuvin 770, Igamoz BZ15, Quimasorb 944, Cromoftal A3R, Bioxid Kronos CL 2220
B	Tinuvin 770, Quimasorb 944, Cromoftal DPP-BO, Cinquasia R RT 891D
C	Tinuvin 770 Igarnoz BZ15, Quimasorb 944, Iagacolor 10401 Bioxid Kronos CL 2220
D	Tinuvin 770, Quimasorb 944, Iagacolor 415, Byferrox 110

The coupled samples A-B and C-D were prepared with different combinations of coloring additives according to the main industrial process. Samples A and B were subjected to artificial aging performed in a xenon test 450 chamber, with a xenon arc lamp as the radiating light source for the simulation of natural aging. The artificial aging

time was 5000 h (equivalent to 2.5 years of natural aging). The samples were labeled as A-5000 and B-5000, respectively. Samples C and D were aged under natural climatic conditions for 2.5 years and were labeled C-2.5 and D-2.5, respectively.

The structural changes and thermal properties of the PP-PE copolymers were measured with FTIR spectrophotometry and DSC techniques. A Nicolet 510M spectrometer with CsI optics was used to obtain the FTIR spectra, with a resolution of 2 cm^{-1} and with an average of 50 scans. Pellets were prepared by the dispersion of the surfaces of finely divided samples (3 mg) in a matrix of KBr (300 mg), followed by compression at 167 MPa.

To determine changes in the FJJR spectra, several authors [14, 18, 20] chose a particular band as a reference to avoid deviations between spectra produced by samples of different weights or thicknesses. The absorption related to this band is known as the reduced or compensated absorption. In this work, the spectral reference band chosen was at 2840 cm^{-1} and was due to methylene symmetric stretching vibrations.

The thermal behavior of the samples was analyzed with DSC. The measurements were made with a Mettler TA4000 thermoanalyzer coupled with a low-temperature (nitrogen coil) DSC 30 apparatus. The calibration of the temperatures and energies was made with standard samples of In, Pb, and Zn under the same conditions used in the sample analysis. The measurements were made with dry air as a purging gas at a flow rate of 20 mL/mm. The heating rate was 10 K/min, a good compromise between the measurement rate and the endothermic melting peak resolution. The sample mass was about 2.5 mg, small enough to prevent the problems caused by heat- and mass-transfer limitations. Several experiments were performed to ensure the reproducibility of the results, with the samples heated to 600, 300, or 185^0C.

The microstructures of the samples were characterized by SEM in a Zeiss DSM 960 A apparatus. The resolution was 3.5 nm, the acceleration voltage was 15 kv, and the working distance was 10-20 mm. The samples were sputtered previously with C with a K 550 Emitech instrument. The aim was to observe microstructural changes arising from the degradation phenomena related to the aging processes, as well as the effects of the thermal treatments applied to the material.

Table 8. Variation of Reduced Absorbance Avarage Values of All Samples as a Funtion of Artificial Aging and Natural Aging.

Wavenumber (cm^{-1})	Functional group	Reduced absorbance average values							
		A	A-5000	B	B-5000	C	C-2.5	D	D-2.5
1740	C═O	0.077	0.083	0.092	0.096	0.109	0.161	0.109	0.118
1735	(ester)	0.075	0.097	0.104	0.097	0.104	0.174	0.104	0.133
1720	C═O	0.059	0.090	0.083	0.096	0.088	0.169	0.088	0.106
1717	(ketone)	0.059	0.097	0.082	0.097	0.088	0.169	0.088	0.105
1167	C—O	0.206	0.212	0.203	0.200	0.250	0.291	0.268	0.276
1650	C═C	0.135	0.109	0.220	0.106	0.201	0.134	0.201	0.182
1460	—CH_2—	1.053	0.994	1.003	0.923	1.273	0.998	1.273	1.173
1378	—CH_3	1.174	1.072	1.117	1.106	1.354	1.146	1.354	1.262
976	Iso-PP	0.251	0.348	0.256	0.303	0.399	0.600	0.467	0.600
901	Iso-PP	0.067	0.085	0.066	0.079	0.082	0.132	0.091	0.132*
812	Iso-PP	0.067	0.108	0.070	0.091	0.091	0.140	0.098	0.140

This band moves to 912 cm^{-1}.

3.2. Results and discussion

We analyzed the characteristic spectral bands of the polymer that were more greatly modified during the aging process. The results are shown in Table 8. The chemical groups related to these bands are carbonyl groups (1735 cm^{-1}), ether (1167 cm^{-1}), nonsaturated bonds (1650 cm^{-1}), methylene (1460 cm^{-1}), and methyl (1378 cm^{-1}). There are also three bands related to the structural characteristics: configuration isomerism and conformational order (812, 901, and 976 cm^{-1}) The evolution of these latter bands allowed us to determine structural and configurational changes.

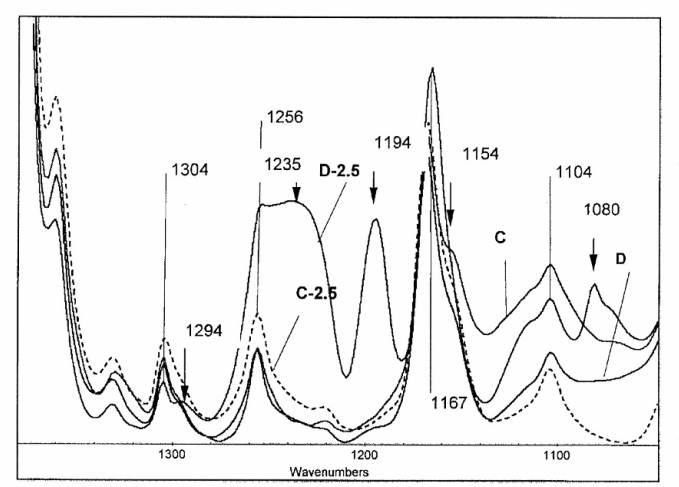

Figure 3. FTIR spectra of samples C and D exposed to natural aging in the spectral range 1025-1380 cm^{-1}

3.2.1. Study of Natural Aging by FTIR

Figure 3 shows the spectral range 1025-1380 cm^{-1} for samples C and D exposed to natural aging. The 1168 cm^{-1} band, associated with the C-O-C group, shows a tendency to increase in aged samples, suggesting the formation of ether groups. Moreover, the FTIR spectrum of sample D-2,5 has three bands at 1235, 1194, and 1080 cm^{-1} (marked by arrows) and two shoulders, one at 1294 cm^{-1} and another at 1154 cm^{-1} (marked by arrows), associated with transitions of the crystalline phase. These spectral differences between the aged and nonaged samples show that the crystallinity of sample D was more affected by the aging process. Sample C was less affected by aging, showing only small spectral changes (the 1235 cm^{-1} band and the shoulder at 1154 cm^{-1}).

Figure 4 shows the spectral range 750-1050 cm^{-1} corresponding to samples C and D not aged and naturally aged. The absorbance of the 812-, 976-, and 998-cm^{-1} bands, related to conformational and configurational changes, is higher in aged samples than in nonaged ones. Moreover, the presence of the bands marked by arrows makes it evident that some changes were produced. The spectral band at 901 cm^{-1} moved to 912

cm^{-1}, and this short shift was attributed to the background changes generated by conformational modifications. Likewise, a small shoulder appears at 941 cm^{-1}, and two peaks appear at 1015 and 1035 cm^{-1} (associated with the stretching vibrations of -C-O-C and –C-O-H, respectively). Both peaks appear as a result of the oxidative process that originated during natural aging.

3.2.2. Study of Artificial Aging by FTIR

Samples A and B were subjected to artificial aging in the xenon test chamber for 5000 h. The spectra of aged and nonaged samples are shown in Figures 5 and 6. The changes detected in both materials (A and B) are very similar. Nevertheless, these changes are not as important as they are for the materials subjected to natural aging for 2.5 years (C and D).

The spectra corresponding to the samples artificially aged (A and B), illustrated in Figure 4, show that degradation phenomena are lower than in the previous case. In the artificially aged samples, only a slight increase in the band absorbances associated with the configuration order was detected. We can conclude, therefore, that exposure to weather leads to more aggressive degradation than that produced by exposure to the homogeneous conditions employed in the xenon test chamber in our study.

3.2.3. Comparison of Natural and Artificial Aging by FTIR

A comparative study of both types of aging processes (natural and artificial) is shown in Figure 7. An increase of the ester and ketone groups (1735 and 1717 cm^{-1}) was detected. This increase was greater in the materials subjected to natural aging. Samples C were the most affected by carbonyl group formation.

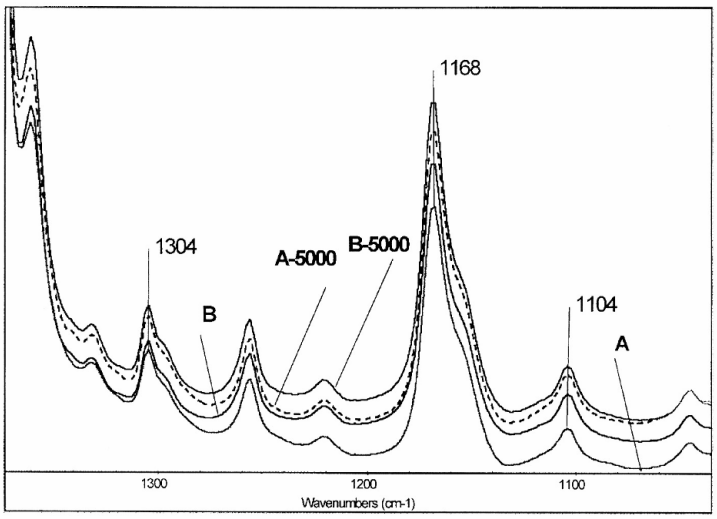

Figure 4 FTIR spectra of samples C and D exposed to natural aging in the spectral range 750-1050 cm^{-1}. Bands marked with arrows are related to large spectral changes.

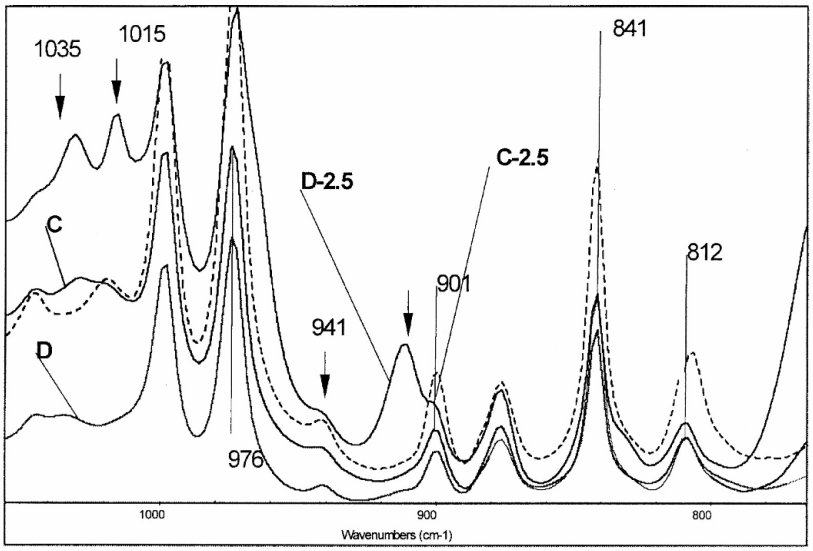

Figure 5 FTIR spectra of samples A and B exposed to artificial aging in the spectral range 1025-1380 cm^{-1}

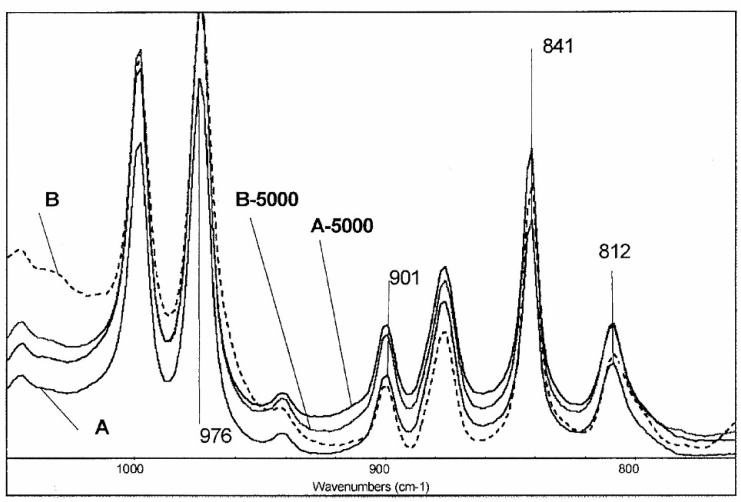

Figure 6 FTIR spectra of samples A and B exposed to artificial aging in the spectral range 750-1050 cm^{-1}. Bands marked with arrows are related to large spectral changes.

Comparing samples C and A (Fig. 7), which only differed in the pigment used and the type of aging, we can observe that natural aging is far more aggressive than artificial aging.

The formation of ether groups related to the 1168-cm^{-1} band (Figs. 3 and 5) is not clear in the artificially aged samples This difference in the evolution of these groups must be influenced by parameters difficult to reproduce in artificial aging in a xenon test chamber (e.g., sudden changes of temperature and humidity, rain, and sea proximity). Furthermore, it is also difficult to reproduce the interactions of these parameters with the pigment used and the ability to react at high temperatures, mainly with sulfurous compounds [21] arising from pollution.

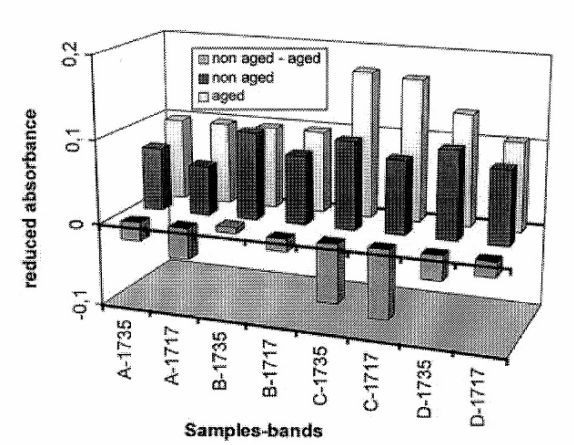

Figure 7 Reduced absorbance results of spectral bands associated with the carbonyl group in all aged samples.

There are several bands related to the double bonds. The one that can best help to define the evolution of the aging process is the 1650-cm^{-1} band, associated with the stretching vibrations of -C=C- The tendency of this band to diminish in the aged samples, as shown in Table 8, is similar in all samples. Nevertheless, it is remarkable that samples artificially aged presented a decrease of 46%; compare this to 33% for the naturally aged ones. The double bonds are generated in the first steps of the aging process, reacting subsequently to produce branching, crosslinking, or both.

The samples exposed to natural aging had a lower percentage of double bonds but higher crosslinking. That is reflected in the configurational changes shown by the evolution of the main bands associated with the tacticity of PP (976, 901, and 812 cm^{-1}) [22] in Figures 4 and 6.

The decline of every band, shown in Figure 8, occurred for all (naturally or artificially) aged samples. The spectral band most sensitive to the changes in the configuration order is the 976-cm^{-1} band, associated with ν(CC) in the chain and with $y_r(CH_3)$.

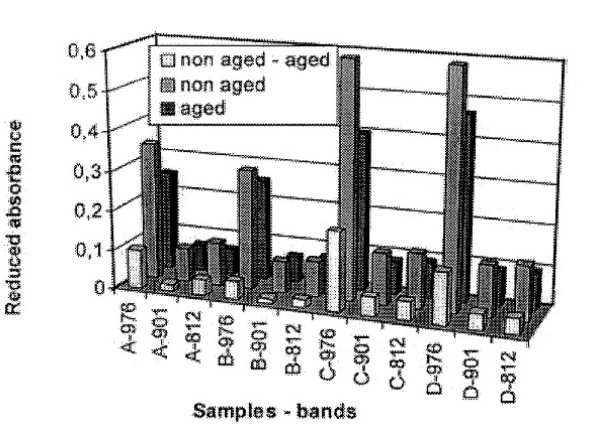

Figure 8 Reduced absorbance corresponding to spectral bands associated with configurational isomerism (976, 901, 812 cm^{-1}) for all aged samples.

Likewise, the tendency of the methyl (1378 cm^{-1}) and methylene (1460 cm^{-1}) groups to diminish was observed in all samples and in both aging processes. The results are given in Figure 9, which shows the evolution of the 1460- and 1378-cm^{-1} bands. The greatest decrease occurred in the naturally aged ones (being more important in C than in D). The breaking of the group combined with the carbon in the natural aging process is widely accepted because this labile carbon easily becomes a free radical through elimination reactions [23, 24] when ultraviolet radiation is present. Moreover, in most of the degradation processes of polyolefins, there is a decrease in the number of methylene groups these phenomena help to confirm that macromolecular chains suffer homolytic and heterolytic breakage [25]. In this work, as shown in the results listed in Table 8 and Figure 9, a methylene decrease was also detected.

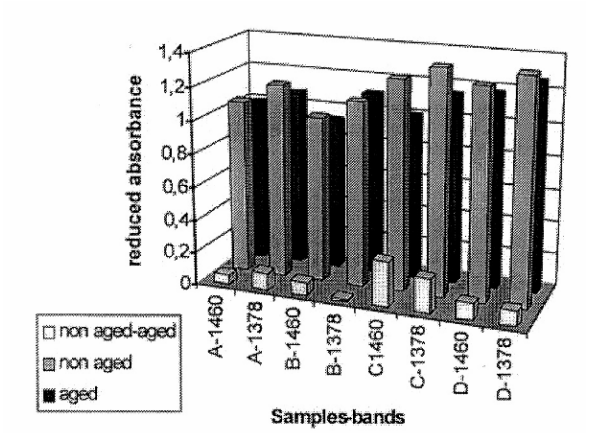

Figure 9 Reduced absorbance corresponding to spectral bands associated with methyl and methylene groups (1460 and 1378 cm^{-1}) for all aged samples

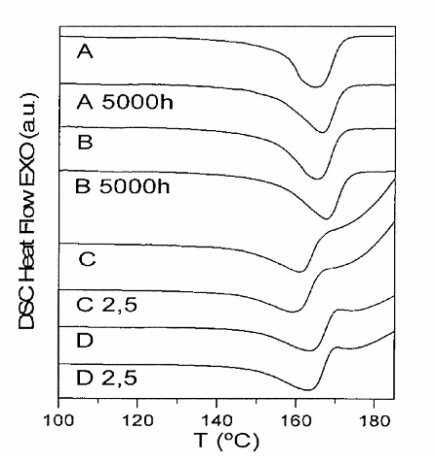

Figure 10 DSC curves corresponding to newly manufactured samples (A, B, C and D) and the aged samples (A-5000, B-5000, C-2.5, and D2.5).

A chain break leads to the generation of terminal methyl groups, of which an increase would be expected, but our data revealed a decrease. This apparent contradiction is due to the fact that the number of methyl groups generated by chain scission is lower than the number of methyl groups that disappear in the formation of free radicals in tertiary carbons. The radicals generated present a high reactivity and provoke the rapid formation of nonsaturated bonds, which act as precursors in the formation of branching and crosslinking processes.

This transformation in the configurational order also appeared in samples A and B, although it was always present as a minor change.

3.2.4. Comparison of Natural and Artificial Aging by DSC and SEM

Figure 10 shows the DSC thermograms of the samples, and Table 9 shows the characteristic thermal parameters of the melting and degradation processes.

In the calorimetric study performed by DSC (heating up to 600^0C), several processes associated with melting and thermal decomposition (beginning after fusion) were detected. As shown in Table 9, the decomposition process of the naturally aged samples (C and D) began at lower temperatures than in other samples. The difference between the melting onset temperature *(T_0)* for the decomposition process of artificially aged samples A and B and the nonaged samples was as low as $1\text{-}2^0$C, whereas the difference was greater for C and D samples (natural aging), being as high as 25-27ºC. These differences also existed in the melting peak temperature *(Tp)* for the melting process. The decrease in the decomposition and melting temperatures is associated with shorter polymeric chains and a lower thermal stability of the material.

In the naturally aged samples (C and D), the melting enthalpy presented a clear decrease (ca. 40%) in comparison with the nonaged ones (Table 9). The enthalpy decrease was intrinsically associated with a loss of the crystalline fraction of the copolymer, as previously shown by FTIR.

Table 9 Characteristics of Melting and Thermal Decomposition Processes

	Melting			Decomposition
Sample	T_o (°C)	T_p (°C)	ΔH (J/g)	T_o (°C)
A	155.0	164.5	81.2	193.5
A-5000	154.1	166.6	69.4	192.0
B	153.7	165.2	75.0	193.1
B-5000	154.9	167.3	72.1	191.2
C	154.1	166.1	73.6	193.8
C-2.5	149.5	161.5	43.6	166.7
D	153.9	166.3	84.4	193.9
D-2.5	150.0	164.0	55.0	169.8

The calorimetric changes detected in the artificially aged samples (A and B) were lower than those observed in naturally aged ones. The melting enthalpy (ΔH) diminished by about 14% in the A samples and by about 4% in the B samples.

Previous studies on the crystallization kinetics of samples A and B led to the conclusion that these processes may be very sensitive to the presence of additives. These results are confirmed in this work through the spectrophotometric and calorimetric studies. Nevertheless, in samples C and D, natural aging produced modifications of a larger magnitude than the use of different additives did.

The superficial morphology of aged samples depends on the type of aging. The surface of the samples aged by weather presented a scale structure, whereas the artificially aged surfaces preserved the original morphology, with the exception of several modified zones.

Another difference was detected when the samples were subjected to a thermal treatment followed by cooling to the crystallization temperature. The structure after the solidification process became porous (Fig. 11, top). Samples A and B, newly manufactured or after aging, presented similar morphologies, without preferential orientations, but the crystallization of samples C and D produced a micelle distribution (Fig. 11, bottom). This difference in behavior is related more to the presence of different additives than to degradation. Additive particles can act as nucleation centers of heterogeneous degradation. It appears that macroscopic structure modifications produced by natural and artificial degradation occur on the surface because an analysis of the internal areas of several broken samples did not show any differences between aged and nonaged samples.

3.3. Conclusions

From the results obtained, it can be stated that natural aging produces configurational and conformational changes of a higher order than artificial aging. Oxidative processes are present in both kinds of aging. The main changes are the formation of carbonyl groups, the scission of hydrocarbonated chains, the formation of free radicals in tertiary carbons, and the initial formation of nonsaturated bonds followed by the progressive participation of these bonds in branching and crosslinking reactions.

The differences in behavior between the samples subjected to the same type of aging could be attributed to the presence of different commercial additives. For sample C, the combination of three types of antioxidants led to a synergistic effect that improved its stability against natural aging. Also, the catalytic effect of some colorants appeared in the results obtained.

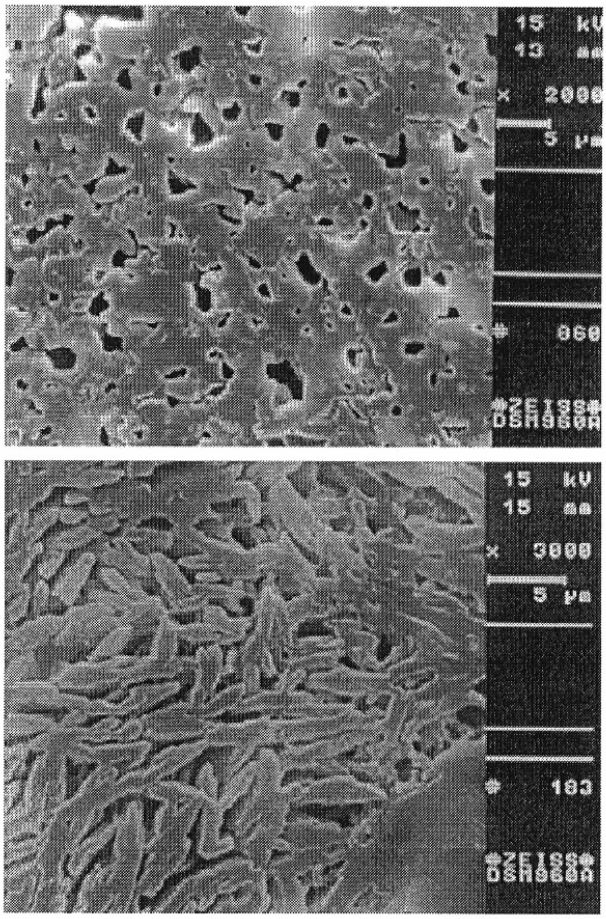

Figure 11 Micrographs corresponding to B-5000 artificial aging (top) and C-2.5 natural aging (bottom).

DSC corroborated several of these results. The Samples naturally aged showed a greater loss of crystallinity than those subjected to the xenon test. The melting enthalpy diminished by about 40% in the naturally aged samples and by only about 14% in the artificially aged samples.

The morphology obtained during the crystallization process was clearly different in samples subjected to both types of aging. This fact could be attributed to the additives used and to the differences between the aging processes.

The intended equivalence between the two types of aging processes has to be reviewed because the heterogeneous conditions in which natural aging occurs (e.g., environment, salinity content, ram, and pollution) produce a greater and more extensive effect than those of the xenon test.

References

1. Tabb, D. L. and Koening, J. L. Macromolecules, 8, 929 (1975).
2. D'Esposito, L. and Koening, J. L. Fourier Transform Infrared Spectroscopy, Vol. 1, Ferraro, J.R. and Basile, L. J. Eds., Academic Press, New York, 1978, p. 73.
3. Musto, P.; Karasaz, F. E. and Macknight, W. J. Polymer, 34(14), 2934 (1993).
4. Delprat, P. and Gardette, J. L. Polymer, 34(5), 903 (1978).
5. Carrasco, F.; Kokta, B. V.; Arnau, J. and Pages, P. Composites, 33(2), 46 (1993).
6. Pagès, P.; Arnau, J.; Carrasco, F.; and Gironés, J. 6th Mediterranean Congr. Chem. Eng., Barcelona, Book of Abstracts, Vol. II, Ed. Departamento de Prensa y Publicaciones, Fira de Barcelona, Barcelona, 1993, p.729.
7. Nikitin, V. N. and Pokrovskii, E. L. Doklady Akad. Nauk SSSR, 95, 109 (1954).
8. Tobbin, M. C. and Carrano, M. J. J Polym. Sci., 24, 93 (1957).
9. Zerbi, G.; Galiano, G.; Fanti, N. D. and Baini, L. Polymer, 30, 2324 (1989).
10. Carrasco, F. Thermochim. Acta, 213, 115 (1993).
11. Alguer, M. S. M. Polymer Science Dictionary, Elsevier, New York, 1989, p. 344.
12. Kaczmarek, H. Polymer 1996, 37, 189.
13. Carrasco, F.; Pagés, P.; Pascual, 8.; Colom, X. Eur Polym J 2001, 37, 1457.
14. Colom, X.; García, T.; Suñol, J J.; Saurina, J.; Carrasco, F. J. Non-Cryst Solids 2001, 287, 308.
15. Esposito, L.; Koening, J. L. In Applications of Fourier Transform Infrared lo Synthetic Polymers and Biological Macromolecules; Ferraro, 1 R.; Basile, L. J., Eds.; Academic: New York, 1978; Vol. 1, Chapter 2.
16. Caykara, T.; Guven, O. Polym Degrad Stab 1999, 65, 225.
17. Chiaotore, O.; Troasarelli, L.; Lazzari, M. Polymer 2000, 41, 1657.
18. Irusta, L.; Fernández-Berridí, M. J. Polymer 1999, 40, 4821.
19. EN 13206:2001; Annex A, Point 8.10.
20. Romeu, J.; Pagès, P.; Carrasco, F. Rev Plást Mod 1997, 74, 255.
21. Schnabel, W. Polymer Degradation Principles and Practical Applications; Hanser: New York, 1981.
22. Bower, D. I.; Maddams, W. F. The Vibrational Spectroscopy of Polymers; Cambridge University Press: Cambridge, England, 1989.
23. Vollhardt, C. Organic Chemislry; Freeman: New York, 1987.
24. Linstromberg, W. W. Organic Chemistry: A Brief Course; Heath: Lexinglon, MA, 1979.
25. Pagès, P.; Carrasco, F.; Saurina, 1.; Colom, X. J Appl Polym Sci 1996, 60, 153.